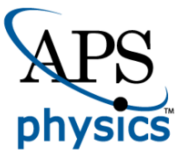

Negative Spin Exchange in a Multielectron Quantum Dot

Frederico Martins, Filip K. Malinowski, Peter D. Nissen, Saeed Fallahi, Geoffrey C. Gardner, Michael J. Manfra, Charles M. Marcus, and Ferdinand Kuemmeth

Phys. Rev. Lett. **119**, 227701 — Published 30 November 2017

DOI: 10.1103/PhysRevLett.119.227701

Negative spin exchange in a multielectron quantum dot

Frederico Martins[1,*], Filip K. Malinowski[1,*], Peter D. Nissen[1], Saeed Fallahi[2], Geoffrey C. Gardner[2], Michael J. Manfra[2,3], Charles M. Marcus[4], Ferdinand Kuemmeth[1]
[1] *Center for Quantum Devices, Niels Bohr Institute, University of Copenhagen, 2100 Copenhagen, Denmark*
[2] *Department of Physics and Astronomy, Station Q Purdue, and Birck Nanotechnology Center, Purdue University, West Lafayette, Indiana 47907, USA*
[3] *School of Electrical and Computer Engineering, and School of Materials Engineering, Purdue University, West Lafayette, Indiana 47907, USA*
[4] *Center for Quantum Devices and Station Q Copenhagen, Niels Bohr Institute, University of Copenhagen, 2100 Copenhagen, Denmark*
[*] *These authors contributed equally to this work*
(Dated: October 30, 2017)

We use a one-electron quantum dot as a spectroscopic probe to study the spin properties of a gate-controlled multielectron GaAs quantum dot at the transition between odd and even occupation number. We observe that the multielectron groundstate transitions from spin-1/2-like to singlet-like to triplet-like as we increase the detuning towards the next higher charge state. The sign reversal in the inferred exchange energy persists at zero magnetic field, and the exchange strength is tunable by gate voltages and in-plane magnetic fields. Complementing spin leakage spectroscopy data, the inspection of coherent multielectron spin exchange oscillations provides further evidence for the sign reversal and, inferentially, for the importance of non-trivial multielectron spin exchange correlations.

PACS numbers: 73.21.La, 03.67.Lx

Semiconducting quantum dots with individual unpaired electronic spins offer a compact platform for quantum computation [1–8]. In these approaches, the essential role of nearest-neighbor interactions poses technological challenges to upscaling, due to the density of electrodes that define and control these quantum circuits [9–13]. This issue has stimulated efforts to study long-range coupling of spin qubits either by electrical dipole-dipole interaction [12–14] or via superconducting microwave cavities [15–17]. However, these approaches involve the charge degree of freedom, which makes the qubit susceptible to electrical noise [18–21]. Alternatively, pulses that induce exchange interactions can be performed fast in a charge-insensitive manner [21–24]. Even though the exchange interaction is intrinsically short-ranged, its range can be increased by means of a quantum mediator [25, 26]. In particular, using a large multielectron quantum dot as an exchange mediator has the potential to do both: provide fast spin interaction [27, 28] and alleviate spatial control line crowding.

Here we investigate a GaAs multielectron quantum dot and show that its spin properties make it suitable for use as a coherent spin mediator. The experiment involves three quantum dots that can be detuned relative to each other using top-gate voltage pulses. The central one-electron dot serves as a probe: its spin can be tunnel coupled either to the left one-electron dot (serving as a reference spin for initialization and readout), or to a large dot on the right, thereby probing its multielectron spin states. We focus on a particular occupancy of the multielectron dot that we find to be odd, $2N+1$, and characterized by an effective spin 1/2. We establish that the exchange coupling between the central probe spin and the multielectron spin depends strongly and non-monotonically on the detuning of relevant gate voltages. Remarkably, this exchange coupling becomes negative, i.e. triplet-preferring, as the central electron is transferred into the right dot. We therefore infer a spin-1 ground state for $2N+2$ occupation, even in the absence of an applied magnetic field. Besides fundamental implications for the role of non-trivial interactions within a multielectron dot, presented elsewhere for a large range of dot occupations [29], our finding has practical applications. For example, the nonmonotonicity of the exchange profile results in a sweet spot at which the exchange splitting has a reduced susceptibility to charge noise. Meanwhile, the sign reversal removes a constraint for the construction of compact dynamically corrected exchange gates [30, 31].

The three quantum dots were fabricated in a $GaAs/Al_{0.3}Ga_{0.7}As$ heterostructure hosting a high mobility two-dimensional electron gas with a bulk density $n = 2.5 \times 10^{15}$ m^{-2}. The confining potential and dot occupancy is voltage-tuned by metallic gates [8, 21]. Figure 1(a) shows the two accumulation gates (colored in green) surrounded by depletion gates, and a schematic cut through the resulting triple-well potential. Gates labeled $V_{L/M/R}$ (colored in red) are connected to high-bandwidth coaxial lines and allow application of nanosecond-scale voltage pulses. An adjacent quantum dot (not shown) serves as a fast charge sensor, i.e. changes in its conductance change the amplitude (V_{RF}) of a reflected rf carrier [32]. All measurements were conducted at base temperature of a dilution refrigerator.

The device can be viewed as a two-electron double

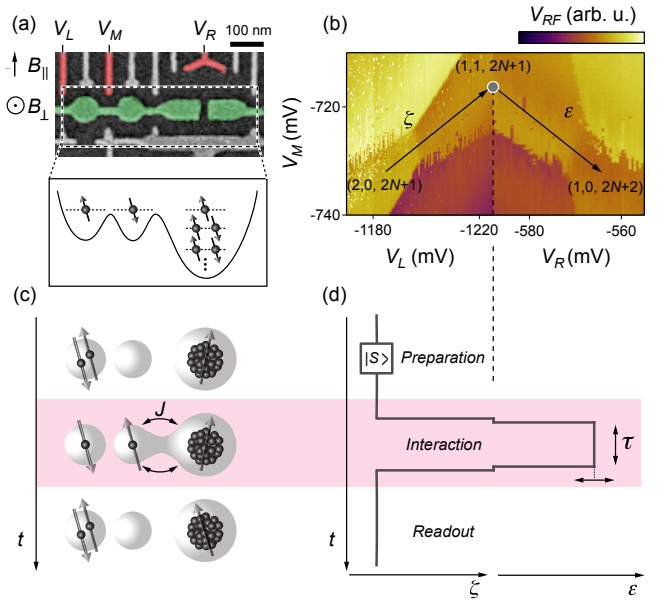

FIG. 1. (a) Electron micrograph of the device consisting of a two-electron double quantum dot next to a multielectron quantum dot. The accumulation gate (colored in green) is operated at positive voltage. Remaining gates deplete the underlying two-dimensional electron gas. Gates $V_{L/M/R}$, highlighted in red, are connected to high-bandwidth lines. (b) Charge diagrams indicating the electron occupation of the triple quantum dot as function of $V_{L/M/R}$. Arrows indicate ζ and ϵ axes in gate voltage space. (c) Concept of the experiment. Two electrons are initialized in a singlet state in the left quantum dot. Thereafter one of the electrons is moved to the middle dot and interacts with the multielectron quantum dot through exchange interaction J. At the end, readout is attained by performing spin-to-charge conversion for two-electron spin states in the double quantum dot. (d) Implementation of the pulse sequence in terms of ζ and ε.

quantum dot (DQD) tunnel-coupled to a multielectron dot (MED) with an estimated number of electrons between 50 and 100, based on n and the area of the MED. By measuring V_{RF} as a function of voltages $V_{L/M/R}$ we map out the dots' occupancies in the vicinity of the charge states (2,0,2N+1), (1,1,2N+1) and (1,0,2N+2). Here, the numbers correspond to electron occupation in the left dot, central dot and the MED, respectively. The resulting charge diagram in Fig. 1(b) allows the definition of two detuning axes in gate-voltage space, ζ and ε, crossing at the point indicated by grey circle. A reduction of ζ pushes the central electron into the left dot, whereas an increase in ε pushes it to the MED (cf. arrows).

The MED spin states are probed by the pulse sequence illustrated in Fig. 1(c,d). First, two electrons are prepared in the left dot in a singlet state, by pulsing to the (2,0,2N+1) charge state. Then a ζ pulse to the (1,1,2N+1) state turns off intra-DQD exchange interactions while maintaining the two-electron spin state. The next step probes the interaction between the central electron and the MED in the vicinity of the charge transition between (1,1,2N+1) and (1,0,2N+2). This is done by pulsing ε, i.e. by temporarily applying a negative voltage pulse to V_M and a positive voltage pulse to V_R. After an interaction time τ we return to (1,1,2N+1) and immediately reduce ζ for single-shot reflectometry readout [33]: If V_{RF} indicates a (2,0,2N+1) charge state, we assign a singlet outcome, whereas (1,1,2N+1) indicates that a spin interaction with the MED has occurred (resulting in a two-electron triplet state, which is spin blocked).

Leakage spectroscopy is performed by choosing τ = 150 ns sufficiently long to detect incoherent spin mixing between the central electron and MED states. Figure 2(a) shows the probability of a singlet outcome, $P_S(\varepsilon, B_\parallel)$, where ε is the detuning voltage during the interaction step and $B_\parallel$ is the applied in-plane magnetic field [see arrow in Fig. 1(a)]. To make connection to the conventional two-electron DQD regime we also plot $P_S(\zeta, B_\parallel)$, acquired by replacing the composite ζ-ε pulse in Fig. 1(d) by a pure ζ pulse. Incoherent leakage from the initialized singlet state is observed as a sharp suppression of P_S for particular detuning values, with a non-trivial magnetic field dependence for $\varepsilon > -5$ mV. To understand this spectrum we note that all features below $\varepsilon \approx -5$ mV are well explained by mixing with fully polarized spin states, consistent with previous spin leakage experiments: The ζ dependence (marked by white triangle) is analogous to mixing between singlet and $|T_+\rangle \equiv |\uparrow\uparrow\rangle$ in two-electron DQDs [7, 9, 34], whereas the ε dependence (blue triangle) is analogues to mixing between a singlet-like state and $|\uparrow\uparrow\uparrow\rangle$ in three-electron triple quantum dots [35]. (Here, each arrow indicates the spin state within one quantum dot.) The characteristic dependence on $B_\parallel$ arises from the Zeeman shift of fully polarized spin states and a non-linear detuning dependence of J [37, 38].

This identification suggests an odd multielectron occupation, i.e. (1,1,2N+1), with effective spin 1/2. Accordingly, we interpret the continuation of the main leakage feature (indicated by a black dot) as the degeneracy point of $|\uparrow\rangle|S\rangle$ and $|\uparrow\uparrow\uparrow\rangle$. In other words, the position of this feature indicates the detuning at which the exchange interaction J equals the Zeeman splitting $|g|\mu_B B_\parallel$ (here $g = -0.44$ is the electronic g-factor for GaAs and μ_B is the Bohr magneton), thereby allowing us to quantify the exchange splitting between the central spin and the effective MED spin [Fig. 2(c)]. Towards higher detuning, $\varepsilon > -5$ mV in Fig 2(a), an overall drop in the background of P_S indicates that the MED ground state transitions into (1,0,2N+2), approximately concurrent with the sharp leakage feature (blue triangle) reaching a maximum before turning towards $B_\parallel = 0$ (black dot). We interpret this maximum as a maximum in the exchange profile, $J(\varepsilon)$, and associate the crossing at $B_\parallel = 0$ with a sign reversal of $J(\varepsilon)$. At $\varepsilon = 0$ two additional leakage features appear at $B_\parallel = 0$. One is nearly field indepen-

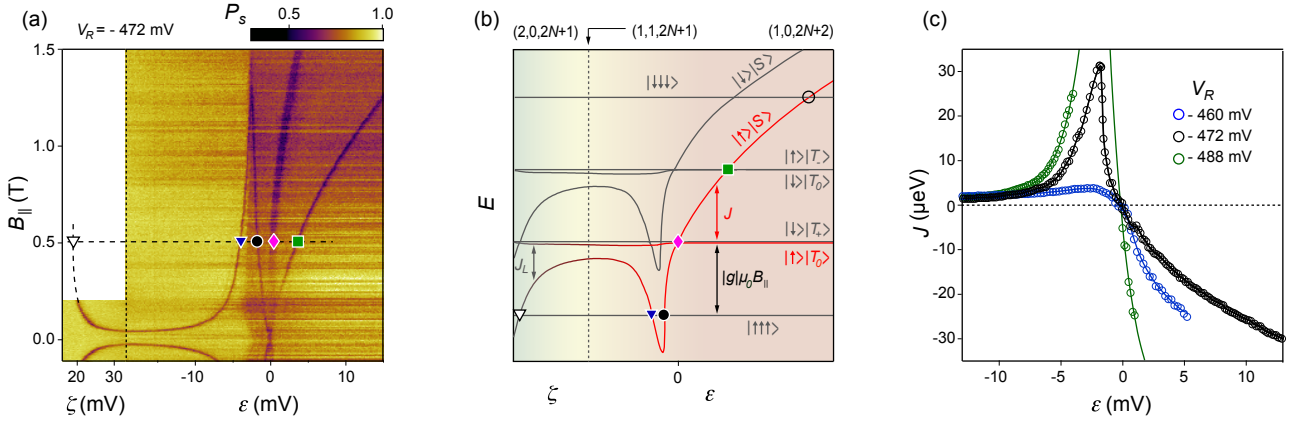

FIG. 2. (a) P_S as a function of ζ, ε and $B_\parallel$ for a fixed, long interaction time $\tau = 150$ ns. Vertical dashed line indicates the crossing of ζ and ε axes in Fig. 1(b). (b) Corresponding energy diagram of the spin states of a Heisenberg model, as a function of ζ, ε for a fixed $B_\parallel$. States highlighted in red witness the interaction between the central probe spin and the effective MED spin, which combine into a singlet-like state, $|\uparrow\rangle|S\rangle$, that is above a triplet-like state, $|\uparrow\rangle|T_0\rangle$, for sufficiently large ε (negative J). The charge character of the ground state transitions from (2,0,2N+1) via (1,1,2N+1) to (1,0,2N+2) as indicated by the background shading. The sign reversal of J happens at $\varepsilon = 0$. The Zeeman shift $|g|\mu_B B_\parallel$ and crossings with other states leading to spin leakage features in (a) are indicated (see main text). Leakage from $|\uparrow\rangle|S\rangle$ to the fully polarized $|\downarrow\downarrow\downarrow\rangle$ state (empty circle) is not observed in (a) because weak Overhauser gradients or spin-orbit coupling do not allow such large changes in spin projection. (c) Experimental exchange profiles for different operating points (distortions of the confining potential), identified by V_R during the readout step (symbols). Black circles are extracted from (a). Solid lines are guides to the eye.

dent (magenta diamond), and hence we associate it with the crossing between $|\uparrow\rangle|S\rangle$ and $|\uparrow\rangle|T_0\rangle$, which has the same spin projection in the direction of magnetic field. The other feature (green square) indicates a crossing with $|\uparrow\rangle|T_-\rangle$. Since the energy of this state increases for larger magnetic field, J must change sign.

To support this analysis by a full spin spectrum, we impose the inferred exchange profile $J(\zeta, \varepsilon)$ from Fig. 2(c) on a Heisenberg model of three spin-1/2 orbitals [39]. The resulting energy diagram, sketched in Fig. 2(b) for finite $B_\parallel$, allows us to identify all characteristic leakage features. On the left side of the energy diagram only tunneling across the left barrier is significant (giving rise to intra-DQD exchange coupling J_L), and the eigenstates are the tensor products of a DQD spin state and a MED "spectator" spin. For example, the white triangle marks the crossing between $|S\rangle|\uparrow\rangle$ and $|\uparrow\uparrow\uparrow\rangle$, and relates the leakage feature in (a) to $J_L(\zeta)$. Analogously, on the right side of the energy diagram, the left dot is decoupled and hosts the spectator spin, while the central spin interacts with the effective MED spin. Here, field dependent crossings map out the positive (blue and black) and negative (green marker) regime of $J(\varepsilon)$. In particular, for crossings of $|\uparrow\rangle|S\rangle$ with $|\uparrow\uparrow\uparrow\rangle$, $|\uparrow\rangle|T_0\rangle$ and $|\uparrow\rangle|T_-\rangle$ rapid mixing is expected to occur [41]. Thereby, the Heisenberg model qualitatively explains all features in the observed leakage spectrum. At high magnetic field, however, the observed leakage feature indicated with a magenta diamond is not field independent as predicted by the model, likely due to orbital coupling of $B_\parallel$ to MED states.

In contrast to three-electron triple dots [35, 36], where

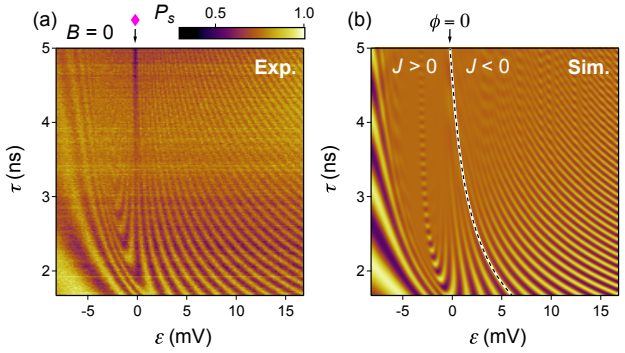

FIG. 3. (a) Exchange oscillations in P_S as a function of ε and exchange time τ, in the vicinity of (1,1,2N+1) and (1,0,2N+2) charge transition. External magnetic field is zero, and DC tuning voltages are the same as in Fig. 2(a) ($V_R = 472$ mV). (b) Simulated exchange oscillations, assuming $J(\varepsilon)$ from Fig. 2(c), Gaussian low-frequency noise in ε with a standard deviation of 0.18 mV, and a rise time of the experimental instrumentation of 0.8 ns. A contour with no net accumulated phase, $\phi = 0$, divides operating regimes where J is positive and negative. Leakage out of the simulated subspace (magenta diamond in (a), see text) was ignored in the simulation.

J is always positive, we observe that $|\uparrow\rangle|S\rangle$ and $|\uparrow\rangle|T_0\rangle$ cross each other at a particular detuning value (which we used to define $\varepsilon = 0$). This implies that the exchange interaction between the single and multielectron quantum dot changes sign from positive to negative, i.e. it is singlet-preferring for small hybridization and

becomes triplet-preferring once the central electron has transferred to the MED. Next, we test for robustness and gate-tunability of this effect. In Fig. 2(c) we plot $J(\varepsilon)$ extracted from Fig. 2(a) (black symbols), and compare it to two exchange profiles (green and blue symbols) measured by distorting the confining potential while preserving the charge configuration of the triple dot system (cf. Supplementary Fig. S1). In all cases $J(\varepsilon)$ shows the same behavior, namely a maximum and sign reversal in the vicinity of the charge transition, and a negative sign in the (1,0,2N+2) configuration. This interpretation implies that the $2N$+2 charge state of the MED has a total spin of 1 at zero magnetic field, which is further confirmed by studying the MED behavior over multiple charge states [29].

Complementary evidence for the sign reversal in J is obtained from time-domain measurements. To this end, we induce coherent exchange oscillations between the central and MED spin by significantly reducing (and varying) the interaction time τ. The observed oscillations are analogous to those observed in exchange-only qubits [36, 37], where the rate of phase accumulation between its two qubit states (i.e. frequency of $P_S(\tau)$) is a measure of the exchange splitting $|J|$. However, the observed pattern of $P_S(\varepsilon,\tau)$, shown in Fig. 3(a) for the same DC tuning parameters as in Fig. 2(a), differ from that of exchange-only qubits. The appearance of a chevron-like pattern around $\varepsilon = -2$ mV indicates the presence of a local maximum in $|J(\varepsilon)|$: Following contours of equal phase (ϕ) around this "sweet spot", we note that for constant τ $\phi(\varepsilon)$ first increases, then decreases. It continues to do so smoothly beyond the $\phi = 0$ contour, implying a sign reversal in $J(\varepsilon)$. Additionally, for large τ a dark feature appears at $\varepsilon = 0$ (magenta diamond), which for $\tau \to 150$ ns turns into the incoherent leakage feature discussed in Fig. 2(a).

To show consistency between time-domain and leakage spectroscopy results, we perform numerical simulations of the exchange oscillations using the measured exchange profile presented in Fig. 2(c). The simulation is limited to the state space with total spin $S = 1/2$ and spin projection $S_z = 1/2$ on the direction of the external magnetic field [indicated with red in Fig. 2(b)] and includes a quasistatic Gaussian noise in ε with standard deviation $\sigma_\epsilon = 0.18$ mV [21, 40] and a rise time of our instrumentation of 0.8 ns. The simulation reproduces a chevron pattern (Fig. 3(b)), whereas simulations using $J(\varepsilon) = |J(\varepsilon)|$ produce a qualitatively different pattern (not shown). Therefore, the contour $\phi = 0$ does indeed separate regions with $J > 0$ from regions with $J < 0$.

Finally, we study the effects of applied magnetic fields on the exchange profile. Figure 4(a) presents P_S as a function of ε and out-of-plane magnetic field $B_\perp$, while keeping $B_\parallel = 0$ and $\tau = 3.33$ ns fixed. In such a plot, contours correspond to constant J in the ε-$B_\perp$ plane, and their curvature indicates that out-of-plane magnetic

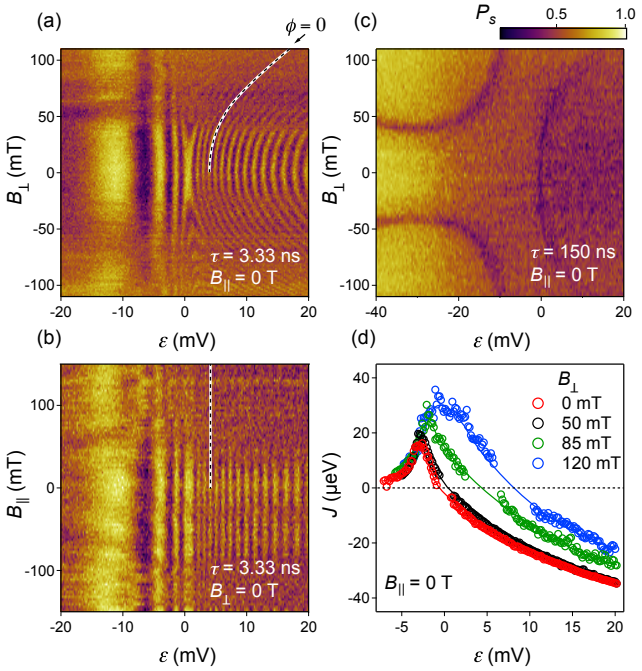

FIG. 4. (a) Exchange oscillations as a function of $B_\perp$ and ε for fixed exchange time $\tau = 3.33$ ns and fixed $B_\parallel = 0$ T. (b) Exchange oscillations as a function of $B_\parallel$ and ε for fixed exchange time $\tau = 3.33$ ns and fixed $B_\perp = 0$ T. (c) Same as (a) but in the leakage spectroscopy regime ($\tau = 150$ ns). Features of reduced P_S correspond to mixing between $|\uparrow\rangle |S\rangle$ and various other states (cf. horizontal cut of Fig. 2(a) at $B_\parallel = 0$). A small deviation between the $J = 0$ feature in (c) and the $\phi = 0$ contour in (a) is likely due the very different values of τ in combination with finite-rise-time effects of our instrumentation. (d) $J(\varepsilon)$ extracted for different values of $B_\perp$.

fields move the sign reversal of J towards higher detuning (cf. $\phi = 0$ contour, marked by a dashed line). For comparison, within the same range, $B_\parallel$ has no observable influence on the pattern of the exchange oscillations (Fig. 4(b)). By choosing τ longer than the coherence time we obtain the $B_\perp$-dependence of the leakage spectrum (Fig. 4(c), using $\tau = 150$ ns). The two leakage features appearing for negative values of ε correspond to mixing between $|\uparrow\rangle |S\rangle$ and the fully polarized $|\uparrow\uparrow\uparrow\rangle$. The leakage feature appearing for positive values of ε indicates $J = 0$; similar to Fig. 2 we expect it to split into three lines at higher fields.

Exchange profiles $J(\varepsilon)$ for $B_\perp = 0$, 50, 85 and 120 mT were extracted from $P_S(\varepsilon,\tau)$ maps obtained for the same tuning voltages as in Fig. 4(a) (Supplementary Fig. S2). Figure 4(d) establishes an electrical sweet spot in $J(\varepsilon)$ that can be precisely tuned by $B_\perp$, hinting at the role of the underlying electronic orbitals. However, their microscopic changes, and associated effects on the exchange profiles, remain outside the scope of our model.

In summary, we have investigated the exchange interaction between a two-electron double quantum dot and

a multielectron dot. We find that the multielectron dot with odd occupation behaves as a spin-1/2 object that gives rise to a non-monotonic exchange coupling to the neighboring dot. By changing the relative dot detuning voltage by a few millivolt the sign of the exchange interaction can be tuned from positive to negative (also at zero magnetic field), indicating the presence of non-trivial electron-electron interactions. Finally, we show that the exchange profile can be tuned by either changing the gate potentials or applying an out-of-plane orbital magnetic field, giving rise to a tunable electrical sweet spot that might benefit the implementation of high-fidelity exchange gates [21, 24] in long-distance quantum mediators.

We thank Edwin Barnes, Stephen Bartlett, Andrew Doherty, and Thomas Smith for helpful discussions. This work was supported by LPS-MPO-CMTC, the EC FP7-ICT project SiSPIN no. 323841, the Army Research Office and the Danish National Research Foundation.

[1] C. Kloeffel and D. Loss, Ann. Rev. Condens. Matter Phys. **4**, 10.1-10.31 (2013).
[2] D. D. Awschalom, L. C. Bassett, A. S. Dzurak, E. L. Hu, J. R. Petta, Science **339**, 1174 (2013).
[3] D. Loss and D. P. DiVincenzo, Phys. Rev. A **57**, 120 (1998).
[4] J. R. Petta, H. Lu and A. C. C. Gossard, Science **327**, 670 (2010).
[5] H. Bluhm, S. Foletti, I. Neder, M. Rudner, D. Mahalu, V. Umansky, and A. Yacoby, Nat. Phys. **7**, 109 (2011).
[6] K. C. Nowack, F. H. L. Koppens, Y. V. Nazarov, L. M. K. Vandersypen, Science **318**, 14301433 (2007).
[7] B. M. Maune, M. G. Borselli, B. Huang, T. D. Ladd, P. W. Deelman, K. S. Holabird, A. A. Kiselev, I. Alvarado-Rodriguez, R. S. Ross, A. E. Schmitz, M. Sokolich, C. A. Watson, M. F. Gyure, and A. T. Hunter, Nature **481** 481, 344347 (2012).
[8] F. K. Malinowski, F. Martins, P. D. Nissen, E. Barnes, M. S. Rudner, S. Fallahi, G. C. Gardner, M. J. Manfra, C. M. Marcus, and F. Kuemmeth, Nat. Nanotechnol., **12**, 1620 (2017).
[9] M. Veldhorst, C. H. Yang, J. C. C. Hwang, W. Huang, J. P. Dehollain, J. T. Muhonen, S. Simmons, A. Laucht, F. E. Hudson, K. M. Itoh, A. Morello and A. S. Dzurak, Nature **526**, 410414 (2015).
[10] D. M. Zajac, T. M. Hazard, X. Mi, E. Nielsen, and J. R. Petta, Applied Physics Letters **6**, 054013 (2016).
[11] T. Ito, T. Otsuka, S. Amaha, M. R. Delbecq, T. Nakajima, J. Yoneda, K. Takeda, G. Allison, A. Noiri, K. Kawasak and S. Tarucha, Scientific Reports **6**, 39113 (2016).
[12] M. D. Shulman, O. E. Dial, S. P. Harvey, H. Bluhm, V. Umansky, and A. Yacoby, Science **336** 202 (2012).
[13] J. M. Nichol, L. A. Orona, S. P. Harvey, S. Fallahi, G. C. Gardner, M. J. Manfra, and A. Yacoby, npj Quantum Information **3**, 3 (2017).
[14] L. Trifunovic, O. Dial, M. Trif, J. R. Wootton, R. Abebe, A. Yacoby and D. Loss, Physical Review X, **2**, 11006 (2012).
[15] X. Mi, J. V. Cady, D. M. Zajac, P. W. Deelman, and J. R. Petta, Science **355**, 156158 (2017).
[16] V. Srinivasa, J. M. Taylor and C. Tahan, Physical Review B **94**, 205421 (2016).
[17] M. Russ and G. Burkard, Phys. Rev. B **91**, 235411 (2015).
[18] W. A. Coish and D. Loss, Physical Review B **72**, 125337 (2005).
[19] J. M. Taylor, J. R., Petta, A. C. Johnson, A. Yacoby, C. M. Marcus and M. D. Lukin, Physical Review B **76**, 35315 (2007).
[20] O. Dial, M. D. Shulman, S. P. Harvey, H. Bluhm, V. Umansky and A. Yacoby, Physical Review Letters **110**, 146804 (2013).
[21] F. Martins F. K. Malinowski, P. D. Nissen, E. Barnes, S. Fallahi, G. C. Gardner, M. J. Manfra, C. M. Marcus, and F. Kuemmeth, Physical Review Letters **116**, 116801 (2016).
[22] K. M. Weiss, J. M. Elzerman, Y. L. Delley, J. Miguel-Sanchez, and A. Imamoglu, Physical Review Letters **109**, 107401 (2012).
[23] B. Bertrand, H. Flentje, S. Takada, M. Yamamoto, S. Tarucha, A. Ludwig, A. D. Wieck, C. Bauerle, and T. Meunier Phys. Rev. Lett. **115**, 096801 (2015).
[24] M. D. Reed, B. M. Maune, R. W. Andrews, M. G. Borselli, K. Eng, M. P. Jura, A.A. Kiselev, T.D. Ladd, S.T. Merkel, I. Milosavljevic, E.J. Pritchett, M.T. Rakher, R.S. Ross, A.E. Schmitz, A. Smith, J.A. Wright, M.F. Gyure, and A.T. Hunter, Physical Review Letters **116**, 110402 (2016).
[25] T. A. Baart, T. Fujita, C. Reichl, W. Wegscheider, and L. M. K. Vandersypen, Nature Nanotechnology **11**, 330334 (2016).
[26] F. Braakman, P. Barthelemy, C. Reichl, W. Wegschneider, and L. M. K. Vandersypen, Nature Nanotechnology **8**, 432437 (2013).
[27] S. Mehl, H. Bluhm, and D. P. Divincenzo, Physical Review B **90**, 045404 (2014).
[28] V. Srinivasa, H. Xu, and J. M. Taylor, Physical Review Letters **114**, 226803 (2015).
[29] F. K. Malinowski, F. Martins, T. B. Smith, S. D. Bartlett, A. C. Doherty, P. D. Nissen, S. Fallahi, G. C. Gardner, M. J. Manfra, C. M. Marcus, and F. Kuemmeth, arXiv:1710.10012 [cond-mat.mes-hall] (2017).
[30] X. Wang, L. S. Bishop, J. P. P. Kestner, E. Barnes, K. Sun, K. and S. Das Sarma, Nature Communications, **3**, 997 (2012).
[31] X. Wang, L. S. Bishop, E. Barnes, J. P. Kestner and S. Das Sarma, Physical Review A **89**, 022310 (2014).
[32] C. Barthel, M. Kjaergaard, J. Medford, M. Stopa, C. M. Marcus, M. P. Hanson, and A. C. Gossard, Physical Review B **81**, 161308R (2010).
[33] C. Barthel, D. J. Reilly, C. M. Marcus, M. P. Hanson, and A. C. Gossard, Physical Review Letters **103**, 160503 (2009).
[34] J. R. Petta, A. C. Johnson, J. M. Taylor, E. A. Laird, A. Yacoby, M. D. Lukin, C. M. Marcus, M. P. Hanson, and A. C. Gossard, Science **309**, 21802184 (2005).
[35] J. Medford, J. Beil, J.M. Taylor, E.I. Rashba, H. Lu, A.C. Gossard, and C.M. Marcus, Physical Review Letters **111**, 050501 (2013).
[36] J. Medford, J. Beil, J. M. Taylor, S. D. Bartlett, A. C. Doherty, E. I. Rashba, D. P. DiVincenzo, H. Lu, A. C.

Gossard, and C. M. Marcus, Nature Nanotechnology **8**, 654 (2013).

[37] E. A. Laird, J. M. Taylor, D. P. DiVincenzo, C. M. Marcus, M. P. Hanson and A. C. Gossard, Physical Review B **82**, 075403 (2010).

[38] J. M. Taylor, V. Srinivasa and J. Medford, Physical Review Letters **111**, 050502 (2013).

[39] The specific detuning dependence of J within a Hubbard model is explained elsewhere [29], and remains phenomenological within this Letter.

[40] E. Barnes, M. S. Rudner, F. Martins, F. K. Malinowski, C. M. Marcus, and F. Kuemmeth, Physical Review B **93**, 121407(R) (2016).

[41] These crossings require a change in electronic spin projections by 1, and hence we expect mixing on a timescale of $T_2^* \approx 10$ ns due to uncontrolled nuclear spin fluctuations and the associated Overhauser gradients [4].